Spectrochimica Acta Part A 78 (2011) 113–121

Contents lists available at ScienceDirect

Spectrochimica Acta Part A: Molecular and Biomolecular Spectroscopy

journal homepage: www.elsevier.com/locate/saa

Molecular structure and vibrational spectra of 2,6-bis(benzylidene)cyclohexanone: A density functional theoretical study

D. Sajan[a,d,*], K. Udaya Lakshmi[b], Y. Erdogdu[c], I. Hubert Joe[d]

[a] Department of Physics, Bishop Moore College, Mavelikara, Alappuzha 690110, Kerala, India
[b] Department of Physics, Saveetha School of Engineering, Saveetha University, Thandalam, Chennai 602105D, India
[c] Department of Physics, Ahi Evran University, 40040 Kirsehir, Turkey
[d] Centre of Molecular and Biophysics Research, Department of Physics, Mar Ivanios College, Thiruvananthapuram 695 015, Kerala, India

ARTICLE INFO

Article history:
Received 13 May 2010
Received in revised form 17 August 2010
Accepted 8 September 2010

Keywords:
Vibrational spectra
NIR-FT Raman
FT-IR
DFT
Conjugation
NBO analysis

ABSTRACT

The near-infrared Fourier transform (NIR-FT) Raman and Fourier transform infrared (FT-IR) spectral analyses of 2,6-bis(benzylidene)cyclohexanone (BBC) molecule, a potential drugs for the treatment of P388 leukemia cells, were carried out along with density functional computations. The optimized geometry of BBC using density functional theory shows that the energetically favored chair conformation is not observed for central cyclohexanone ring and is found to possess a nearly 'half chair' conformation and shows less expansion of the angles and more rotation about the bonds. The existence of intramolecular C–H···O improper, blue-shifted hydrogen bond was investigated by means of the NBO analysis. The lowering of carbonyl stretching vibration can be attributed to the mesomeric effect and the π-orbital conjugation induced by the unsaturation in the α-carbon atoms and co-planarity of the (–CH=C–(C=O)–C=CH–) group.

1. Introduction

The cyclo-conjugated bis(benzylidene)ketone families of compounds have undergone intensive research, owing to their higher cytotoxicity towards P388 leukemia cells compared to other clinically useful drugs [1]. The enhancements of bioactivity upon the substitution of methylene group and dimethyl amino group to the above compounds have been reported [2]. Vibrational spectroscopic studies of cyclohexanone and its derivatives have been reported earlier [3–6]. The Raman optical activity features of cyclohexanone derivatives have been studied using Raman spectral bands and normal coordinate analysis [7,8]. IR and Raman spectral investigations of 2,6-bis(p-N,N-dimethyl benzylidene)cyclohexanone [9], 2,6-bis(p-methoxy benzylidene)cyclohexanone [10] and 2,6-bis(p-methyl benzylidene)cyclohexanone [11], supported by *ab initio* density functional theory studies have been reported. Though the crystal structure of the title compound, 2,6-bis(benzylidene)cyclohexanone (BBC) has been reported [2,12], the vibrational spectral features of BBC crystal have not been subject of detailed analysis so far. NIR-FT Raman spectroscopy combined with quantum chemical computations have recently been used as effective tools in the vibrational analysis of drug molecules, biological compounds, natural products and NLO active compounds [13–15] since fluorescence free Raman spectra and computed results can help unambiguous identification of vibrational modes as well as the bonding and structural features of complex organic molecular systems. The present work reports the detailed vibrational spectral analysis of 2,6-bis(benzylidene)cyclohexanone molecule (Fig. 1) to elucidate the correlation between the molecular structure and prediction of normal modes, to understand the structural and bonding features, steric effect, the intramolecular interactions and factors influencing the vibrational spectrum of the molecule supported using the scaled quantum mechanical (SQM) force field technique based on density functional theory.

2. Experimental

BBC has been synthesized, as described by Zongchao et al. [8]. The IR spectrum was recorded on a Perkin-Elmer Spectrum One FT-IR spectrometer. The spectral resolution was 1 cm^{-1}. The standard KBr technique with 1 mg of sample per 300 mg of KBr was used. The Raman spectrum was recorded on a Bruker RFS100/S near-infrared Fourier transform (NIR-FT) instrument equipped with an FRA106 Raman module. An Nd:YAG laser at 1064 nm with an output on

* Corresponding author at: Department of Physics, Bishop Moore College, Mavelikara, Alappuzha 690110, Kerala, India. Tel.: +91 9495043765; fax: +91 4792303230.
E-mail address: dsajand@gmail.com (D. Sajan).

1386-1425/$ – see front matter © 2010 Elsevier B.V. All rights reserved.
doi:10.1016/j.saa.2010.09.007

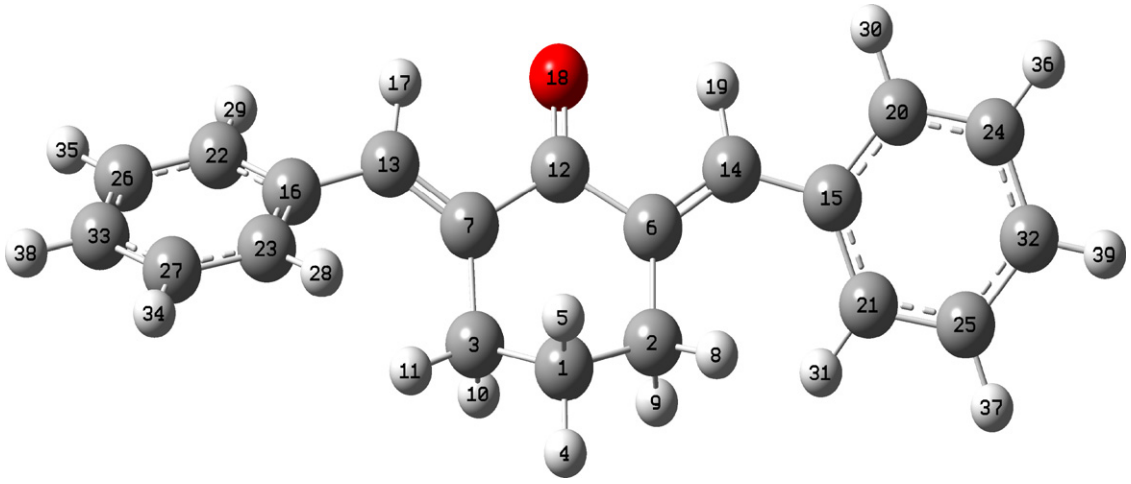

Fig. 1. Optimized molecular structure of BBC calculated at B3LYP/6-311G(d,p).

300 mW was used for excitation. The detector was a Ge diode cooled to liquid nitrogen temperature; 1000 scans were accumulated with a total registration time of about 30 min. The spectral resolution after apodization was 2 cm^{-1}. A correction according to the fourth-power scattering factor was performed, but no correction was made to the instrumental response. The upper limit for the Raman shift is 3500 cm^{-1} owing to the detector sensitivity and the lower Raman shift limit is around 10 cm^{-1} owing to the Rayleigh line cut-off by a notch filter.

3. Computational details

Density functional theoretical (DFT) computations have been performed at the B3LYP/6-311G(d,p) level to derive the optimized geometry and vibrational wavenumbers of normal modes of BBC using Gaussian '03 program package [16]. Molecular geometries were fully optimized by Berny's optimization algorithm using redundant internal coordinates. All optimized structures were confirmed to be minimum energy conformations. Harmonic vibrational wavenumbers were calculated using analytic second derivatives to confirm the convergence to minima on the potential surface and to evaluate the zero-point vibrational energies (ZPVE). At the optimized structure of the BBC, no imaginary frequency modes were obtained, proving that a true minimum on the potential energy surface was found. The optimum geometry was determined by minimizing the energy with respect to all geometrical parameters without imposing molecular symmetry constraints. The inclusion of '*d*' polarization and double-zeta function in the split valance basis set is expected to produce a marked improvement in the calculated geometry [17]. The DFT hybrid B3LYP functional tends also to overestimate the fundamental modes in comparison to the other DFT methods, therefore scaling factor *s* has to be used for obtaining a considerably better agreement with experimental data. The calculated wavenumbers are scaled by an empirical factor of 0.9613 [18] to account for systematic errors caused by basis set incompleteness, neglect of electron correlation and vibrational anharmonicity. The vibrational modes were assigned on the basis of PED analysis using SQM program [19]. Normal coordinate analysis of the title molecules has been carried out to obtain a more complete description of the molecular motions involved in the fundamentals.

The Raman activities (S_i) calculated by the Gaussian '03 program have been converted to relative Raman intensities (I_i) using the following relationship derived from the basic theory of Raman scattering [20].

$$I_i = \frac{f(\nu_o - \nu_i)^4 S_i}{\nu_i \left[1 - \exp(-hc\nu_i/kT)\right]} \quad (1)$$

where ν_o is the exciting frequency (in cm^{-1} units), ν_i is the vibrational wavenumber of the *i*th normal mode, *h*, *c* and *k* are universal constants, and *f* is the suitably chosen common scaling factor for all the peak intensities.

4. Results and discussion

4.1. Crystal structure

BBC crystallizes in space group $P2_{1/c}$. From the single crystal XRD data [2,12] it is observed that the crystal belongs to monoclinic system with the following cell dimensions: $a = 9.5087$ Å, $b = 18.5431$ Å, $c = 9.6523$ Å with $\beta = 116^\circ$.

4.2. Optimized geometry

The calculated structural parameters for BBC are listed in Table 1. The available X-ray diffraction values are also given in the table for comparison. Among the different conformers of cyclohexanone, the chair form is energetically favored [21]. The computed values of torsion angles C_6–C_2–C_1–C_3, C_2–C_1–C_3–C_7, C_1–C_3–C_7–C_{12}, C_3–C_7–C_{12}–C_6, C_{12}–C_6–C_2–C_1 and C_2–C_6–C_{12}–C_7 are 54.1°, −61.8°, 39.9°, −10.5°, −24.9° and 2.7° respectively. The low values of C_3–C_7–C_{12}–C_6 and C_2–C_6–C_{12}–C_7 reveal a distorted chair form for the central cyclohexanone ring in BBC and can be concluded that the chair form arises due to the van der Waals' repulsion between the hydrogen atoms belonging to neighboring carbon atoms. But the absence of hydrogen atoms in C_6, C_{12} and C_7 positions reduces the chair formation, giving a nearly 'half chair' structure for the central ring. The presence of van der Waals repulsion is confirmed by the computed values of intramolecular non-bonded distances $H_8 \cdots H_{31}$ and $H_{10} \cdots H_{28}$ respectively equal to 2.13 and 2.15 Å. In order to reduce the steric repulsion the bond angles are expanded C_2–C_6–C_{14}, C_6–C_{14}–C_{15}, C_{14}–C_{15}–C_{21}, C_3–C_7–C_{13}, C_7–C_{13}–C_{16} and C_{13}–C_{16}–C_{23} at 124.9°, 130.8°, 124.7°,126.3°, 129.9° and 123.5° respectively. The rotation about C_{14}–C_{15} and C_{13}–C_{16} bonds at the expense of the conjugation energy of the system. The reduction in the values of bond angles H_{19}–C_{14}–C_6 and C_7–C_{13}–H_{17} from their expected values has been enhanced by non-bonded interactions

Table 1
Optimized geometric data for BBC using B3LYP/6-311G (d,p).

Bond length (Å)	Values		Bond angle (°)	Values		Torsion angle (°)	Values	
	B3LYP/6-311G (d,p)	X-ray [2]		B3LYP/6-311G(d,p)	X-ray [2]		B3LYP/6-311G (d,p)	X-ray [2]
$C_2–C_1$	1.53	1.53	$C_2–C_1–C_3$	109.9	11.2	$C_3–C_1–C_2–C_6$	54.1	–
$C_1–C_3$	1.53	1.52	$C_2–C_1–H_4$	109.6	–	$C_3–C_7–C_{12}–C_6$	−10.5	–
$C_1–H_4$	1.09	–	$C_2–C_1–H_5$	110.1	–	$C_3–C_1–C_2–H_9$	−67.5	–
$C_1–H_5$	1.09	–	$C_1–C_2–C_6$	112.9	110.3	$C_6–C_2–C_1–H_4$	175.5	–
$C_2–C_6$	1.52	1.51	$C_1–C_2–H_8$	110.2	–	$C_6–C_2–C_1–H_5$	−67.0	–
$C_2–H_8$	1.09	–	$C_1–C_2–H_9$	107.8	–	$C_2–C_1–C_3–C_7$	−61.8	–
$C_2–H_9$	1.10	–	$C_1–C_3–C_7$	111.1	112.7	$C_2–C_1–C_3–H_{10}$	57.3	–
$C_3–C_7$	1.51	1.51	$C_1–C_3–H_{10}$	108.1	–	$C_2–C_1–C_3–H_{11}$	173.3	–
$C_3–H_{10}$	1.10	–	$C_1–C_3–H_{11}$	111.5	–	$C_1–C_2–C_6–C_{12}$	−24.9	–
$C_3–H_{11}$	1.09	–	$C_2–C_6–C_{12}$	119.8	117.8	$C_1–C_2–C_6–C_{14}$	152.5	–
$C_6–C_{12}$	1.51	1.50	$C_2–C_6–C_{14}$	124.9	125.5	$C_1–C_3–C_7–C_{12}$	39.9	−41.0
$C_6–C_{14}$	1.36	1.34	$C_3–C_7–C_{12}$	117.8	118.9	$C_1–C_3–C_7–C_{13}$	142.1	–
$C_7–C_{12}$	1.51	1.50	$C_3–C_7–C_{13}$	126.3	125.5	$C_2–C_6–C_{12}–C_7$	2.7	28.5
$C_7–C_{13}$	1.35	1.34	$C_6–C_{12}–C_7$	118.6	119.0	$C_2–C_6–C_{12}–O_{18}$	−178.8	–
$C_{12}–O_{18}$	1.23	1.23	$C_6–C_{12}–O_{18}$	120.7	120.0	$C_2–C_6–C_{14}–C_{15}$	2.46	5.9
$C_{13}–C_{16}$	1.47	1.47	$C_7–C_{13}–C_{16}$	129.9	130.5	$C_2–C_6–C_{14}–H_{19}$	−175.5	–
$C_{13}–H_{17}$	1.09	–	$C_7–C_{13}–H_{17}$	114.7	–	$C_3–C_7–C_{12}–C_6$	−10.5	–
$C_{14}–C_{15}$	1.46	1.47	$C_6–C_{14}–C_{15}$	130.8	129.0	$C_3–C_7–C_{13}–C_{16}$	4.1	−0.5
$C_{14}–H_{19}$	1.09	–	$C_6–C_{14}–H_{19}$	114.4	–	$C_3–C_7–C_{13}–H_{17}$	−173.6	–
$C_{15}–C_{20}$	1.41	1.40	$C_{14}–C_{15}–C_{21}$	124.7	123.0	$C_7–C_{13}–C_{16}–C_{22}$	32.3	–
$C_{15}–C_{21}$	1.41	1.40	$C_{13}–C_{16}–C_{22}$	118.4	117.3	$C_7–C_{13}–C_{16}–C_{23}$	43.9	−28.7
$C_{16}–C_{22}$	1.41	1.38	$C_{13}–C_{16}–C_{23}$	123.5	–	$C_6–C_{14}–C_{15}–C_{20}$	−154.9	–
$C_{16}–C_{23}$	1.41	1.40	$C_{15}–C_{20}–C_{24}$	121.4	120.7	$C_6–C_{14}–C_{15}–C_{21}$	−23.1	40.1
$C_{20}–C_{24}$	1.39	1.38	$C_{15}–C_{20}–H_{30}$	118.8	–	$C_{14}–C_{15}–C_{20}–C_{24}$	179.7	–
$C_{20}–H_{30}$	1.09	–	$C_{15}–C_{21}–C_{25}$	120.9	120.8	$C_{14}–C_{15}–C_{20}–H_{30}$	0.35	–
$C_{21}–C_{25}$	1.39	1.38	$C_{15}–C_{21}–H_{31}$	119.8	–	$C_{21}–C_{15}–C_{20}–C_{24}$	−2.1	–
$C_{21}–H_{31}$	1.08	–	$C_{16}–C_{22}–C_{26}$	121.1	121.2	$C_{13}–C_{16}–C_{22}–C_{26}$	−179.5	–
$C_{22}–C_{26}$	1.39	1.38	$C_{16}–C_{22}–H_{29}$	119.1	–	$C_{14}–C_{16}–C_{22}–H_{29}$	1.3	–
$C_{22}–H_{29}$	1.09	–	$C_{16}–C_{23}–C_{27}$	120.8	120.3	$C_{13}–C_{16}–C_{23}–C_{27}$	178.8	–
$C_{23}–C_{27}$	1.39	1.40	$C_{27}–C_{23}–H_{28}$	119.5	–	$C_{13}–C_{16}–C_{23}–C_{28}$	1.13	–
$C_{23}–H_{28}$	1.09	–	$C_{20}–C_{24}–C_{32}$	120.0	120.5	$C_{16}–C_{22}–C_{26}–C_{33}$	1.42	–
$C_{24}–C_{32}$	1.39	138	$C_{21}–C_{24}–H_{36}$	119.8	–	$C_{16}–C_{22}–C_{26}–H_{35}$	−179.1	–
$C_{24}–H_{36}$	1.09	–	$C_{21}–C_{25}–C_{32}$	120.4	120.6	$C_{16}–C_{23}–C_{27}–C_{33}$	0.12	–
$C_{25}–C_{32}$	1.39	1.38	$C_{21}–C_{25}–H_{37}$	119.5	–	$C_{16}–C_{23}–C_{27}–H_{34}$	−179.4	–
$C_{25}–H_{37}$	1.09	–	$C_{22}–C_{26}–C_{33}$	120.1	119.9	$C_{22}–C_{26}–C_{33}–C_{27}$	−0.91	–
$C_{26}–C_{33}$	1.39	1.39	$C_{23}–C_{27}–C_{33}$	120.4	120.4	$C_{22}–C_{26}–C_{33}–H_{38}$	0.33	–
$C_{26}–H_{35}$	1.08	–	$C_{23}–C_{27}–H_{34}$	119.6	–	$C_{23}–C_{27}–C_{33}–C_{26}$	179.4	–
$C_{27}–C_{33}$	1.39	1.38	$C_{24}–C_{32}–C_{25}$	119.5	119.5	$C_{12}–C_6–C_{14}–H_{19}$	−2.8	–
$C_{27}–H_{34}$	1.08	–	$C_{24}–C_{35}–H_{39}$	120.2	–	$C_{14}–C_6–C_{12}–O_{18}$	3.1	–
$C_{32}–H_{39}$	1.08	–	$C_{26}–C_{33}–C_{27}$	119.5	119.9	$C_{13}–C_7–C_{12}–O_{18}$	−7.1	–
$C_{33}–H_{38}$	1.08	–	$C_{13}–C_{16}–C_{23}$	123.5	124.5	$C_{12}–C_7–C_{13}–H_{17}$	43.0	–
$C_{16}–C_{23}$	1.41	1.40	$C_{26}–C_{33}–H_{38}$	120.3	–	$C_3–C_7–C_{12}–C_6$	39.9	–

$H_{17}\cdots O_{18}$ and $O_{18}\cdots H_{19}$, whose values have been computed as 2.24 and 2.25 Å respectively (Table 2).

The DFT calculation predicts the tilting of phenyl ring planes Ph1 ($C_6–C_{14}–C_{15}–C_{21}$) and Ph2 ($C_7–C_{13}–C_{16}–C_{23}$) to 27.0° and −43.9° respectively with respect to the dienone moiety. This is attributed to the steric repulsion between the aromatic rings and the central ring and also due to the van der Walls' repulsion between the aryl and aliphatic hydrogen atoms. This is evident from the short intramolecular non-bonded $H_8\cdots H_{31}$, $H_{11}\cdots H_{28}$, $H_{17}\cdots H_{29}$, and $H_{19}\cdots H_{30}$ distances respectively equal to 2.217, 2.147, 2.533 and 2.364 Å respectively. This is analyzed by relaxed PES scanning calculations in which the torsion angle $C_6–C_{14}–C_{15}–C_{21}$ and $C_7–C_{13}–C_{16}–C_{23}$ is varied from 0° to 360° with a step size of 10° and the resulting energy profile (Fig. 2). The rotation of Ph1 about $C_{14}–C_{15}$ and Ph2 about $C_{13}–C_{16}$ bonds at the expense of the conjugation energy of the system is another way to minimize the van der Walls' repulsion.

Table 2
Some intramolecular non-bonded distances in BBC at B3LYP/6-311G(d,p) level.

Parameter	Value
$C_1\cdots C_{13}$	3.726
$C_1\cdots C_{14}$	3.790
$O_{18}\cdots C_{13}$	2.734
$O_{18}\cdots C_{14}$	2.721
$C_{13}\cdots C_{14}$	4.836
$C_{32}\cdots C_{33}$	13.145
$O_{18}\cdots H_{19}$	2.247
$H_{19}\cdots H_{30}$	2.364
$O_{18}\cdots H_{17}$	2.274
$H_{17}\cdots H_{29}$	2.533
$H_8\cdots H_{31}$	2.17
$H_9\cdots H_{31}$	2.353
$H_{11}\cdots H_{28}$	2.147

The effects of steric interaction on the geometry of BBC can be obtained from the results of relaxed PES scan which reveal that an increase of torsion angle $C_6–C_{14}–C_{15}–C_{21}$ directly affects CH_2, C=O and bridge moieties. Variation of the geometrical parameters associated with these moieties can be observed from the results of PES scan and can be attributed to the variation in the van der Waals interactions $H_{31}\cdots H_8$ and $H_{30}\cdots H_{19}$ responsible for ring twisting, as $C_6–C_{14}–C_{15}–C_{21}$ moves to energetically favorable value. This, in turn, affects ring geometry causing an increase of bond angle $C_{25}–C_{21}–H_{31}$ and reduction in bond angle $C_{21}–C_{15}–C_{14}$. The variation of $C_6–C_{14}–C_{15}–C_{21}$ affecting the geometry of bridge can be observed from the remarkable variation of torsion angle $C_{20}–C_{15}–C_{14}–H_{19}$ along with slight variation in the angles $C_{15}–C_{14}–H_{19}$ and $C_{15}–C_{14}–C_6$. Also, the influence on carbonyl group can be understood by the large variation in $C_2–C_6–C_{12}–O_{18}$ and that on the CH_2 group can be noticed by the substantial variation in the torsional values of $C_{12}–C_6–C_2–H_9$ and $C_{12}–C_6–C_2–H_8$.

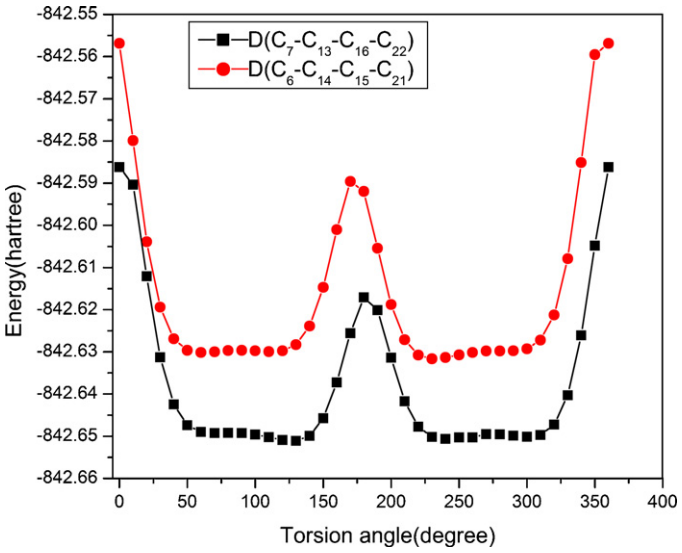

Fig. 2. Result of relaxed potential energy surface scan torsion angle of phenyl ring w.r.t. bridge.

The variation in the torsion angle C_7–C_{13}–C_{16}–C_{23} is found to cause changes in the geometrical parameters of ring, bridge, CH_2 and C=O groups. With the variation of the torsion angle C_7–C_{13}–C_{16}–C_{23} changes in the torsional value of C_1–C_3–C_7–C_{12} can be observed which indicates that the ring twisting directly enhances the twisting of the central cyclohexanone ring, influencing the formation of chair conformation. The changes in the CH_2 geometry are revealed by the changes in the torsional value of C_2–C_1–C_3–H_{10} while the ring geometry perturbation can be observed from the enhancement of angle C_{27}–C_{23}–H_{28}. The carbonyl group is influenced by the ring twisting, from the observed changes in C_3–C_7–C_{12}–O_{18} and the geometrical changes of the bridge (between Ph2 and cyclohexanone) can be found from the remarkable variation in H_7–C_{13}–C_{16}–C_{22} and slight variation in the angles C_3–C_7–C_{13}, C_3–C_7–H_{17}, C_7–C_{13}–C_{16} and C_{13}–C_{16}–C_{22}.

4.3. NBO analysis

NBO analysis provides an efficient method for investigating CT or conjugative interaction in molecular systems. Some electron donor orbital, acceptor orbital and the interacting stabilization energy resulting from the second-order micro-disturbance theory have been reported [22] .The larger the $E(2)$ value, the more intensive is the interaction between electron donors and electron acceptors, i.e. the more donating tendency from electron donors to electron acceptors and the greater the extent of conjugation of the whole system. DFT level computation is used to investigate the various second-order interactions between the filled orbitals of one subsystem and vacant orbitals of another subsystem, which is a measure of the delocalization or hyperconjugation [23]. The main natural orbital interactions were analyzed with the NBO 5.0 program [24]. The hyperconjugative interaction energy was deduced from the second-order perturbation approach

$$E(2) = -n_\sigma \frac{\langle \sigma|F|\sigma\rangle^2}{\varepsilon_{\sigma^*} - \varepsilon_\sigma} = -n_\sigma \frac{F_{ij}^2}{\Delta E} \quad (2)$$

where $\langle \sigma|F|\sigma\rangle^2$ or F_{ij}^2 is the Fock matrix element between the i and j NBO orbitals, ε_σ and ε_{σ^*} are the energies of σ and σ* NBO's, and n_σ is the population of the donor σ orbital.

The second-order perturbation theory analysis of Fock matrix in the NBO basis of the molecule shows strong intramolecular hyperconjugative interactions, which are presented in Table 3. The stabilization energy $E(2)$ associated with hyperconjugative interactions $n_2(O_{18}) \rightarrow \sigma^*(C_{13}–H_{17})$ and $n_2(O_{18}) \rightarrow \sigma^*(C_{14}–H_{19})$ are obtained as 4.77 and 4.73 kJ mol^{-1} respectively (Table 3) which quantify the extend of intramolecular hydrogen bonding. The differences in $E(2)$ energies are reasonably due to the fact that the accumulation of electron density in the C–H bond is not only drawn from the $n(O)$ of hydrogen-acceptor but also from the entire molecule. The orbital interaction energy for $n(LP_2O_{18}) \rightarrow \sigma^*(C_6–C_{12})$ is 81.38 kJ mol^{-1} and $n(LP_2O_{18}) \rightarrow \pi^*(C_7–C_{12})$ is 80.25 kJ mol^{-1} which are higher values than the other devocalizations. These ICTs around the rings can induce large bioactivity in the molecule. The p-character of the oxygen lone pair orbitals [$LP_2(O_{18})$] and [$LP_1(O_{18})$] is 99.99% and 43.3% respectively (Table 3). Thus, a very close to pure π-type lone pair orbital participates in electron donation to the σ*(C–O) orbital for the $LP_2(O_{18}) \rightarrow \sigma^*(C_{12}–O_{18})$ interaction in the molecule.

In the last few years, the role of the weak C–H···O interactions, crystal engineering and molecular recognition processes has aroused considerable interest, owing to their anomalous behaviour [25]. Although the C–H···O interactions are considered weak in nature, they form 20–25% of the total number of hydrogen bonds constituting the second most important group [26]. These interactions have shown to be of greater importance in biological systems in order to elucidate the structure–activity relationship [27]. The *ab initio* calculations have been particularly useful in the identification of C–H···O hydrogen bonds in which the C–H donor group is strengthened, shortened, and blue-shifted (up-shifted) in stretching vibrational wavenumber [28]. The intramolecular contacts $H_{17}\cdots O_{18}$ and $H_{19}\cdots O_{18}$ occur with H···O distances 2.273 and 2.247 Å respectively, which are significantly shorter than that of the van der Waals separation between the O atom and the H atom (2.72 Å) [25], indicating the possibility of the intramolecular C–H···O interaction in BBC. The calculated C–H···O angle 104.1°, for both interactions, is well within the angle limit as the interaction path is not necessarily be linear [29]. The DFT calculation predicts the shortening of C_{13}–H_{17} and C_{14}–H_{19} bonds by ~0.005 Å while C=O is elongated. The contraction in the C_{13}–H_{17} and C_{14}–H_{19} bonds leads to blue shift in the calculated vibrational wavenumber with a decrease in intensity. The strengthening and contraction of C–H bonds is due to rehybridization [30], which is revealed by the low value of electron density (0.02156*e* and 0.02155*e*) in the σ* C_{13}–H_{17} and σ* C_{14}–H_{19} orbitals respectively.

The Mulliken population analysis in the BBC molecule was calculated using the B3LYP/6-311G(d,p) level. The charge distribution structure of BBC is shown in Fig. 3. The oxygen (O_{18}) atom has more negative charges, whereas the carbon atom C_{12} and hydrogen (H_{17} and H_{19}) has more positive charge than the other carbon and hydrogen atoms. The result suggests that the atoms bonded to the carbon atom and all oxygen atoms are electron acceptor and the charge transfer takes place from C to O.

In BBC molecule various weak interactions, such as C–H···O intermolecular hydrogen-bonding interactions are manifested and play an important role in determining stability of the molecule. The presence of carbonyl group leads to the electronic coupling between ring π-electrons and oxygen lone pair electrons which provide stabilization to the molecular structure and enhance its bioactivity. Hence it is of importance to study the electrostatic potential distribution in the molecule. The molecular electrostatic potential (MEP) is a property that the electrons and nuclei of a molecule create at each point r in the surrounding space [31]. ESP serves as a useful quantity to explain hydrogen bonding, reactivity and structure–activity relationship of molecules and correlates with dipole moment, electro negativity, partial charges and site of chemical reactivity of the molecule. It provides a visual method to understand the relative polarity of a molecule. The regions with negative MEP correspond to the areas of high electron density, representing a strong attraction between the proton and the points on

Table 3
Second-order perturbation theory analysis of Fock matrix in NBO basis.

Lone pair	Occupancy	Donor–acceptor interaction	Hybrid (% p-character)	$E(2)$[a] (kJ mol^{-1})	$E(j)-E(i)$[b] (a.u.)	$F(i,j)$[c] (a.u.)
LP_1O_{18}	1.9769	$n(LP_1O_{18})\rightarrow\sigma^*(C_6–C_{12})$	$SP^{0.73}$(43.3)	7.657	4.644	0.1715
		$n(LP_1O_{18})\rightarrow\sigma^*(C_7–C_{12})$		7.489	4.644	0.1674
LP_2O_{18}	1.8773	$n(LP_2O_{18})\rightarrow\sigma^*(C_6–C_{12})$	$SP^{1.0}$(99.99)	81.38	2.845	0.4351
		$n(LP_2O_{18})\rightarrow\sigma^*(C_7–C_{12})$		80.25	4.1	0.431
		$n(LP_2O_{18})\rightarrow\sigma^*(C_{13}–H_{17})$		4.77	3.012	0.1088
		$n(LP_2O_{18})\rightarrow\sigma^*(C_{14}–H_{19})$		4.703	3.012	0.113

[a] $E(2)$ means energy of hyperconjugative interactions; *cf.* Eq. (2).
[b] Energy difference between donor and acceptor i and j NBO orbitals.
[c] $F(i,j)$ is the Fock matrix element between i and j NBO orbitals.

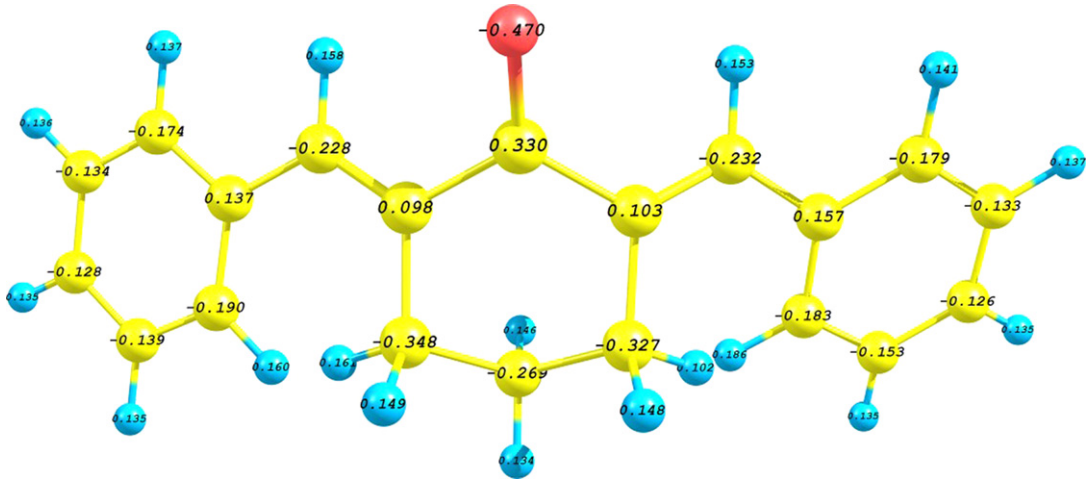

Fig. 3. The Mulliken charge distribution of BBC calculated at the B3LYP/6-311G(d,p) level of theory.

the molecular surface, have the brightest red color and for the positive valued regions, areas of lowest electron density, have deep blue to indigo color, indicating the regions of maximum repulsion. The electron density isosurface on to which the electrostatic potential surface has been mapped is shown in Fig. 4 for BBC. The different values of the electrostatic potential at the surface are represented by different colors; red represents regions of most negative electrostatic potential, blue represents regions of most positive electrostatic potential and green represents regions of zero potential. From Fig. 4, it is visible that the region of the most negative electrostatic potential is spread over the O_{18} atom of the carbonyl group. This indicates the delocalization of π-electrons over the carbonyl group. This also reveals extended conjugation of the cyclohexanone ring with the carbonyl group. (For interpretation of the references to color in this paragraph, the reader is referred to the web version of the article.)

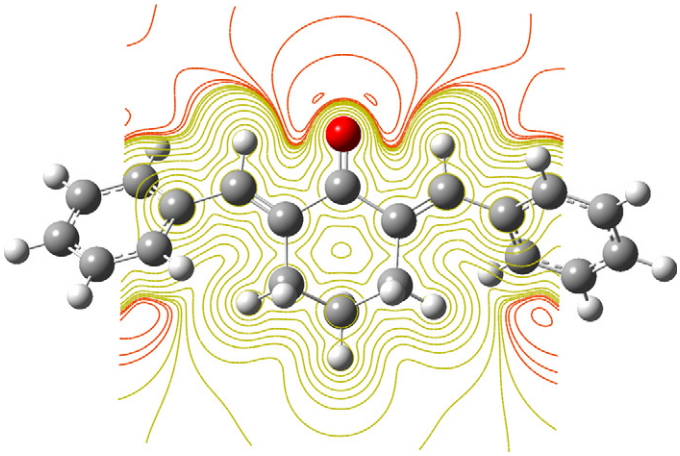

Fig. 4. Molecular electrostatic potential mapped on the isodensity surface for BBC calculated at the B3LYP/6-311G(d, p) level of theory.

4.4. HOMO–LUMO energy

The conjugated molecules are characterized by a small highest occupied molecular orbital–lowest unoccupied molecular orbital (HOMO–LUMO) separation, which is the result of a significant degree of ICT from the end-capping electron-donor groups to the efficient electron-acceptor groups through π-conjugated path [32]. The atomic orbital compositions of the frontier molecular orbital are sketched in Fig. 5. The HOMO–LUMO energy gap of BBC was calculated at the B3LYP/6-311(d,p) level, which reveals that the energy gap reflects the chemical activity of the molecule. The LUMO as an electron acceptor represents the ability to obtain an electron, and HOMO represents the ability to donate an electron. The calculated self-consistent field (SCF) energy of BBC is −848.1752 a.u. The calculated energy value of HOMO is −9.4976 eV and LUMO is −6.4679 eV. The energy gap (−3.027 eV) of HOMO–LUMO explains the eventual charge transfer interaction within the molecule, which influences the biological activity of the molecule. Consequently, the lowering of the HOMO–LUMO band gap is essentially a consequence of the large stabilization of the LUMO due to the strong electron-acceptor ability of the electron-acceptor group.

4.5. Vibrational spectral analysis

The vibrational analysis of BBC is performed on the basis of the characteristic vibrations of cyclohexanone and phenyl ring modes. The computed vibrational wavenumbers and the atomic displace-

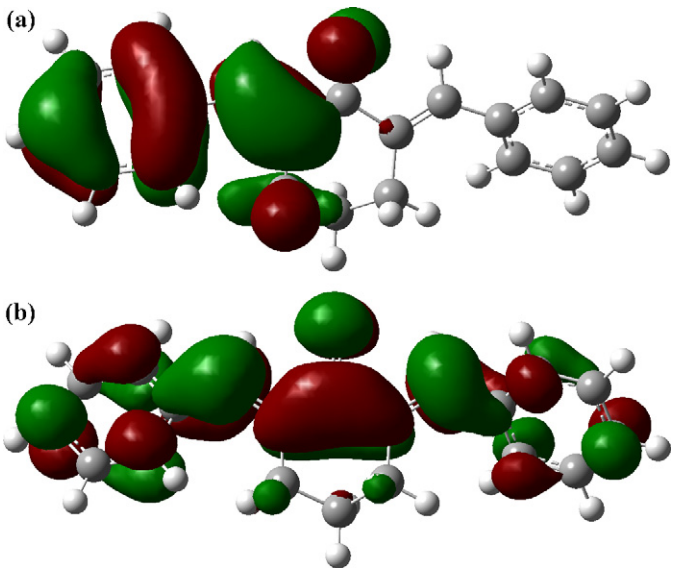

Fig. 5. (a) HOMO plot of BBC at B3LYP/6-311G(d,p) and (b) LUMO plot of BBC at B3LYP/6-311G(d,p).

ments corresponding to the different normal modes are used for identifying the vibrational modes unambiguously. The assignments of phenyl vibrations are made according to Wilson's numbering convention [33]. The calculated vibrational wavenumbers, measured infrared and Raman band positions and their assignments are given in Table 4. The observed and simulated FT-IR and Raman spectra of BBC are given in Figs. 6 and 7

4.5.1. Phenyl ring vibrations

The C–H stretching vibrations in the benzene derivatives arise from three non-degenerate modes a_{1g} (3072 cm^{-1}), b_{1u} (3060 cm^{-1}) and two degenerate mode e_{2g} (3047 cm^{-1}), e_{1u} (3099 cm^{-1}), i.e. vibrations 2, 7, 13, 20a and 20b respectively. The aromatic C–H stretching [34–37] vibrations in monosubstituted benzene rings are generally observed in the region 3000–3100 cm^{-1}. In the IR spectra the bands at 3082, 3058, and 3022 cm^{-1} are assigned of benzene mode 20a, 2 and 20b. The modes 2 and 20b of benzene are identified in Raman spectrum at 3060 and 3024 cm^{-1} respectively. A comparison with the results from the normal mode analysis of BBC shows that the aromatic C–H stretching vibrations around 3050 cm^{-1} remain unaltered by cyclohexanone substitution. All the aromatic CH stretching bands are found to be weak and this is due to the decrease of dipole moment caused by the reduction of negative charge on the carbon atom. This reduction occurs because of the electron withdrawal on the carbon atom by the substituent due to the decrease of inductive effect, which in turn is caused by the increased chain length of the substituent [38].

The quadrant stretching (mode 8) and semicircle stretching (mode 19) of C–C bonds of benzene ring has two doubly degenerate modes, e_{2g} and b_{1u} which are found around 1596 and 1485 cm^{-1} respectively [33–37]. The wavenumber of vibrational pair 8 in monosubstituted benzenes is rather insensitive of substitution. The actual band positions of these modes are determined by the position of the substitution around the ring and not so much by the nature of the substituents [33–37]. The phenyl ring mode 8a manifests as intense bands in IR and Raman spectra at 1607 and 1596 cm^{-1} respectively. The 8b mode can be found as intense bands in infrared spectrum at 1574 cm^{-1} and in Raman at 1567 cm^{-1}. The vibrational modes 19a and 19b are computed at 1485 and 1454 cm^{-1} respectively. The strong band at 1485 cm^{-1} in IR corresponds to the ring mode 19a.The phenyl ring mode 19b can be observed as a strong band at 1443 cm^{-1} in IR spectrum and the corresponding band in Raman are very weak at 1447 cm^{-1}.The vibrational mode 8 and 19 interact a little with C–H in plane bending, hydrogen and its carbon moving oppositely, but the substitutents are nearly motionless which are supported by computed results. A comparison with results from the normal mode analysis of phenyl ring shows that the ring mode around 1620–1400 cm^{-1} remains unaltered by heavy substitution [33]. The band position and the vibrational form of the ring stretching mode 14 of BBC correlate with that of other monosubstituted benzenes [39] and is insensitive to substituent or coupling effects. A very strong band in IR at 1301 cm^{-1} has contributions from the ring mode 14.

The C–H in plane bending vibrations appears in the region 1300–1000 cm^{-1}. Among the CH in plane bending modes 3, 9a, 15, 18a and 18b allowed are active for the monosubstituted phenyl ring [33]. The vibrational mode 18a can be observed at 1034 cm^{-1} in Raman and at 1031 cm^{-1} in IR. The intense IR band at 1169 cm^{-1}

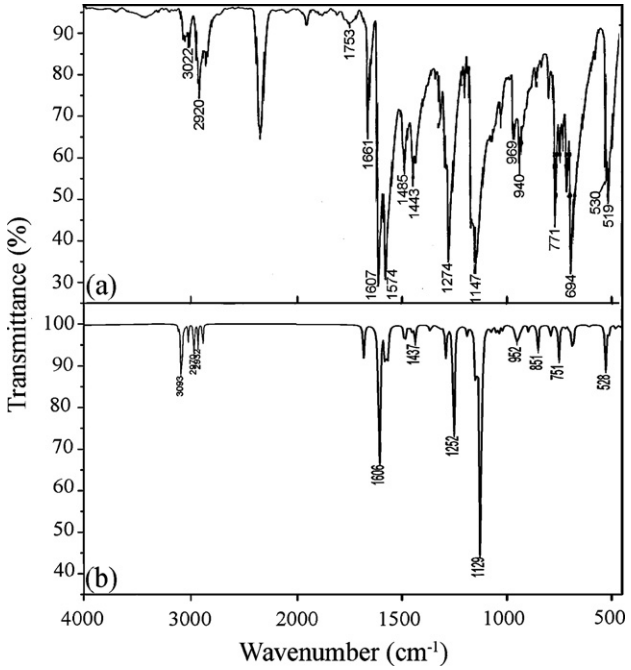

Fig. 6. (a) FT-IR spectra of BBC and (b) simulated IR spectra of BBC.

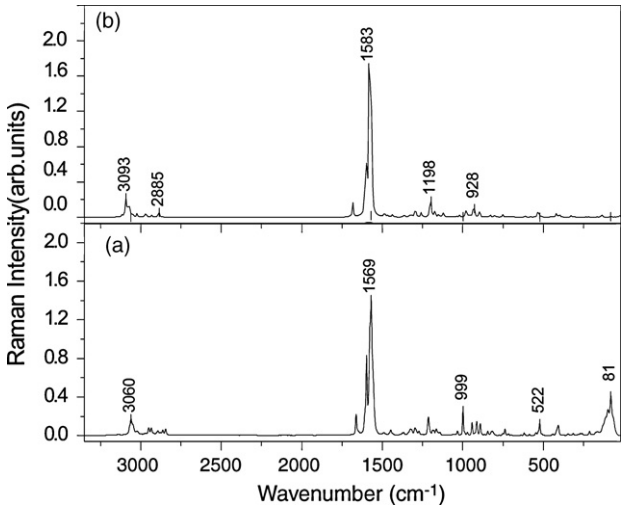

Fig. 7. (a) FT-Raman spectra of BBC and (b) simulated Raman spectra of BBC.

Table 4
Calculated vibrational wavenumbers, measured IR and Raman band positions (cm^{-1}) and assignments for BBC.

Experimental		Computational B3LYP /6-311G (d,p) scaled				PED (%)	Assignment
ν_{IR} (cm^{-1})	$\Delta\nu_{Raman}$ (cm^{-1})	ν_{cal} (cm^{-1})	Relative intensity		ρ		
			IR	Raman			
3082 w		3093	4.8	1.34	0.29	$\upsilon_{CH}(98)$	20a, CH stretch
3058 w	3060 m	3064	0.13	0.08	0.20	$\upsilon_{CH}(99)$	2, CH stretch
3022 m	3024 m	3018	8.51	0.48	0.52	$\upsilon_{CH}(98)$	20b, CH stretch
2962 m	2952 m	2967	13.2	0.38	0.69	$\upsilon_{CH}(98)$	CH_2 (C_1) asym. stretch
2934 m	2934 m	2942	8.57	0.38	0.75	$\upsilon_{CH}(95)$	CH_2 (C_2) asym. stretch
2920 m	2922 wsh	2926	10.2	0.48	0.02	$\upsilon_{CH}(100)$	CH_2 (C_3) asym. stretch
2890 m	2895 m	2889	9.14	0.25	0.20	$\upsilon_{CH}(99)$	CH_2 (C_1) sym. stretch
2862 m	2863 m	2879	3.7	0.77	0.52	$\upsilon_{CH}(97)$	CH_2 (C_3) sym. stretch
2843 m	2846	2854	2.4	0.27	0.69	$\upsilon_{CH}(94)$	CH_2 (C_2) sym. stretch
1662 m	1662 m	1680	15.1	5.07	0.75	$\upsilon_{OC}(55)+\upsilon_{CC}(25)$	CO stretch
1607 vvs		1606	91.5	10.26	0.02	$\upsilon_{CC}(68)$	8a, ring stretch
	1596 m	1596	0.9	14.6	0.02	$\upsilon_{CC}(59)$	8a, ring stretch
1574 vvs	1567 vs	1583	25.2	100.0	0.31	$\upsilon_{CC}(64)+\delta_{CCH}(15)$	8b, ring stretch
1485 s		1485	6.23	0.95	0.02	$\upsilon_{CC}(30)+\delta_{CCH}(69)$	19a, ring stretch + deformation
1443 s	1447 vw	1454	0.25	0.12	0.46	$\delta_{HCH}(29)+\Gamma_{CCCH}(31)+\Gamma_{HCCH(}19)$	19b, ring stretch + deformation
1434 s	1431 vw	1439	0.63	0.9	0.47	$\upsilon_{CC}(30)+\delta_{CCH}(49)$	CH_2 scissoring
1340 w		1340	0.25	0.3	0.53	$\delta_{CCH}(37)+\Gamma_{CCCH}(10)+\Gamma_{HCCH}(15)$	CH_2 wagging
1315 m		1332	0.67	0.72	0.49	$\upsilon_{CC}(50)$	14, ring stretch
1274 vs		1298	3.98	4.57	0.75	$\delta_{CCH}(33)$	9b, CH deformation + CH_2 twisting
1203 m	1213 w	1198	0.07	14.36	0.74	$\upsilon_{CC}(18)+\delta_{CCH}(75)$	CH_2 twisting
1187 w		1180	4.37	2.37	0.40	$\upsilon_{CC}(15)+\delta_{CCH}(70)$	CH_2 twisting
1169 s		1176	0.34	1.65	0.61	$\upsilon_{CC}(18)+\delta_{CCH}(75)$	9a, CH deformation
1147 vs		1148	38.4	0.31	0.44	$\upsilon_{CC}(15)+\delta_{CCH}(13)+\Gamma_{HCCH(}36)$	15, CH deformation
1031 m	1034 w	1034	100	0.43	0.27	$\delta_{CCH}(12)+\Gamma_{HCCH}(33)$	18a, CH deformation + CH_2 rocking
	999 s	1018	0.8	3.32	0.44	$\upsilon_{CC}(34)+\delta_{CCC}(42)$	1, ring breath
969 m		977	0.69	4.41	0.48	$\Gamma_{CCCH}(12)+\Gamma_{HCCH}(50)$	17a, CH deformation
940 m	943 s	944	5.69	0.25	0.16	$\upsilon_{CC}(10)+\delta_{OCC}(11)+\Gamma_{CCCH}(15)$	Ring stretch of cyclohexanone
	914 m	928	0.08	11.6	0.75	$\Gamma_{CCCH}(55)$	17b, CH deformation
	892 m	896	2.59	2.43	0.58	CCC(11)	CH_2 ip rocking
864 w		852	11.9	0.24	0.64	$\Gamma_{CCCH}(16)+\Gamma_{HCCH}(14)$	$C_{(13,14)}H_{(17,19)}$ deformation
839 w	844 w	832	0.21	1.24	0.75	$\delta_{CCH}(14)+\Gamma_{HCCH}(12)+\Gamma_{CCCH}(21)$	10a, CH deformation
	815 w	811	0.07	1.11	0.75	$\Gamma_{CCCH}(96)$	CH deformation
804 m		804	0.01	1.86	0.10	CC(50) + CCC(10)	10b, CH deformation
771 s		792	3.67	0.92	0.75	$\Gamma_{CCCH}(44)$	CH deformation
750 m	752 w	753	10.5	1.71	0.75	$\Gamma_{CCCH}(39)$	CH deformation
736 m	737 m	725	7.23	0.72	0.75	$\delta_{CCC}(32)+\Gamma_{CCCH}(43)$	C–C–C bend + CH deformation
694 vs		685	9.02	0.13	0.74	$\Gamma_{CCCC}(38)+\Gamma_{CCCH}(47)$	11, CH deformation
666 s		662	0.14	0.08	0.70	$\Gamma_{CCCC}(37)+\Gamma_{CCCH}(49)$	CH deformation
	620 w	614	0.40	0.47	0.75	$\delta_{CCC}(25)$	6b, ring deformation
584 w	587 w	578	0.05	0.35	0.75	$\upsilon_{CC}(15)+\delta_{CCC}(35)$	6a, ring deformation
	545w	535	0.55	9.9	0.19	$\upsilon_{CC}(13)+\delta_{OCC}(17)+\Gamma_{CCCH}(20)$	CH deformation
530 s		522	20.4	2.18	0.38	$\upsilon_{CC}(11)+\delta_{OCC}(17)+\Gamma_{CCCH}(24)$	16a, ring deformation
519 s	523 m	513	4.05	0.78	0.38	$\Gamma_{CCCC}(38)+\Gamma_{CCCH}(25)$	16b, ring deformation
	442 w	457	1.21	0.4	0.72	$\delta_{CCC}(23)+\Gamma_{CCCC}(10)$	CCC bend of cyclohexanone ring

is assigned to 9a of benzene. The vibrational mode 9b of benzene is observed as a strong IR band at 1274 cm^{-1}. The strong IR band at 1147 cm^{-1} is attributed to vibration 15.

The absorption bands arising from C–H out-of-plane bending vibrations are usually observed in the region at 1000–675 cm^{-1} [33–37]. The C–H out-of-plane bending vibration 17a are observed as a strong band in IR at 969 cm^{-1} and Raman active mode 17b can be observed as medium band in Raman spectrum at 914 cm^{-1}. The modes corresponding to 10a is observed as weak band at 844 and 839 cm^{-1} in Raman and IR respectively. The intense IR band at 694 cm^{-1} is assigned to C–H out-of-plane bending mode, 11 of benzene.

The ring breathing vibrations are generally very strong in Raman spectrum. Normal vibration 1 of phenyl ring is usually referred to as a substitutent sensitive vibration [33–37]. For a heavy substitution these modes found in the region 1100–1000 cm^{-1} are strongly Raman active. This is confirmed by the strong intense Raman band at 999 cm^{-1} which is supported by computed results. The phenyl ring modes 6a, 6b, 16a and 16b can be observed in expected region are shown in Table 4.

4.5.2. Vibrations of cyclohexanone

The vibrations belonging to cyclohexanone ring in the stretching region correspond to CH_2 asymmetric and symmetric stretching vibrations are observed separately both in IR and in Raman as medium intense bands at 2962, 2934, 2920, 2890, 2862, 2843 and 2952, 2934, 2922, 2895, 2863, 2846 cm^{-1} respectively. Down shifting of $C_3H_{10,11}$ and $C_2H_{8,9}$ stretching vibrational modes are due to the steric interaction between the aromatic rings and the central ring, which is justified by DFT computations also.

The spectral distinction between CH_2 groups involving C_2 and that involving C_1 and C_3 can be observed for bending vibrations. The scissoring vibrations involving C_2 and C_3 can be observed in IR band at 1434 cm^{-1} and weak Raman band at 1431 cm^{-1} respectively. Other wagging vibrations are mixed with the CH in plane bending vibrations of the bridge and CH_2 twisting. The CH_2 twisting modes involving C_1 and C_2 and that involving C_3 are observed as weak bands in IR spectra at 1274 and 1203 cm^{-1} respectively, while the later mode is coupled with the C–H in plane bending vibrations. The band at 1187 and 1031 cm^{-1} in IR spectrum has contributions from CH_2 twisting.

In order to assess the dependence of spectral modes of BBC on the conformation of central cyclohexanone ring, it is compared with Raman, IR [9–11] and computed spectra of cyclohexanone which possesses a chair conformation. The chair conformation is evident from the computed values of torsion angles, 54.1°, −61.8°, 39.9°, −10.5°, −24.9° and 2.7° respectively for C_6–C_2–C_1–C_3, C_2–C_1–C_3–C_7, C_1–C_3–C_7–C_{12}, C_3–C_7–C_{12}–C_6, C_{12}–C_6–C_2–C_1 and C_2–C_6–C_{12}–C_7 computed using DFT at 3LYP/6-311G(d,p) level. For cyclohexanone, the computed carbonyl stretching wavenumber can be found at 1748 cm^{-1} while strong IR and Raman bands can be observed at 1708 and 1705 cm^{-1} respectively, lowered due to association in the solid phase [27]. But 'half chaired' cyclohexanone ring of BBC produces carbonyl stretching band at 1662 cm^{-1} in both IR and Raman where the computed value is 1680 cm^{-1}. The computed normal mode shows that the C=O group is not vibrating independently, but as a group (–CH=C–(C=O)–C=CH–) and the band position of the carbonyl stretching in the lower wavenumber, than expected, can be attributed to the symmetric vibration of the above group. The alternate π-orbitals lead to mesomeric interaction for the above group, making it to act as a single spectral unit [9–11], which is evident from the strong coupling of C=O stretch, C_7–C_{13} stretch, C_{14}–H_{15} bend and C_6–C_{14} stretches in the in plane bending region. The lowering can be attributed to the expanded conjugation [40–42] induced by the unsaturation of the α-carbon atoms C_7 and C_6. The conjugation is enhanced here due to the maximum overlap of π-orbitals, occurring due to the planarity of the group (–CH=C–(C=O)–C=CH–). The co-planarity of the group is evident from the torsion angles H_{19}–C_{14}–C_6–C_{12}, C_{14}–C_6–C_{12}–O_{18}, O_{18}–C_{12}–C_7–C_{13} and H_{17}–C_{13}–C_7–C_{12} whose DFT values are respectively equal to −2.88°, 3.15°, −7.1° and 43.0°. Here the planarity is not hindered by the possible steric effects, because of the heavy substitutions in C_7 and C_6 positions.

The lowering of carbonyl stretching wavenumber can also be explained in terms of bond angle effects, i.e. the increase of C–C(=O)–C angle reduces the carbonyl stretching wavenumber [9–11,42]. This can be explained as: when C=O stretch occurs, adjacent C–C bond contracts whose restoring force has component in the direction of C=O restoring force and it cooperates with C=O restoring force, where the extent of cooperation being dependent on C–C(=O)–C angle and, in turn, C=O stretching wavenumber. In BBC, the DFT value of C–C(=O)–C bond angle is 118.8° while for cyclohexanone the corresponding angle is 115.1°, which is also responsible for the observed difference in C=O stretching force constants.

In cyclohexanone, the C=O in plane bending vibration can be observed as a strong band in IR at 491 cm^{-1} and as a weak band in Raman at 493 cm^{-1} [9–11,27]. But the C=O in plane bending is absent in BBC. Also, C–C–C bend of the cyclohexanone ring in BBC can be observed as medium in IR at 736 cm^{-1}, medium band in Raman at 737 cm^{-1} and as strong band in IR at 519 cm^{-1} which are mixed with the bending vibrations of the bridge and phenyl rings. But, the C–C–C bend in the cyclohexanone ring can be observed at lower wavenumber, i.e. 442 cm^{-1} in Raman. For other bands, the spectral distinction between chaired cyclohexanone and half chaired cyclohexanone in BBC is difficult because of the mixing of cyclohexanone vibrations with that of phenyl rings and bridges.

5. Conclusions

NIR-FT Raman and FT-IR spectra of the crystallized 2,6-bis(benzylidene)cyclohexanone have been recorded and analyzed using density functional theory. The optimized geometry of BBC using density functional theory shows that the energetically favored chair conformation is not observed for central cyclohexanone ring and is found to possess a nearly 'half chair' conformation and shows less expansion of the angles and more rotation about the bonds. The van der Waals interaction between H_{30} and H_{19} causes the steric interaction, resulting in the twisting of phenyl ring Ph1 and the ring twisting of Ph2 is caused by the van der Waals repulsions, $H_{11}\cdots H_{28}$ and $H_{17}\cdots H_{29}$. The existence of intramolecular C–H···O improper, blue-shifted hydrogen bond was investigated by means of the NBO analysis. The vibrational analysis reveals that the methylene groups involving C_2 and C_3, taking part in steric interaction, show different spectral behaviours compared to the CH_2 group involving C_1 and this spectral distinction can be observed for both stretching and deformation modes. The lowering of carbonyl stretching vibration can be attributed to the mesomeric effect and the π-orbital conjugation induced by the unsaturation in the α-carbon atoms and co-planarity of the group (–CH=C–(C=O)–C=CH–).

References

[1] L. Liu, S. Liu, X. Chen, L. Guo, Y. Che, Bioorg. Med. Chem. 17 (2009) 606–613.
[2] Z. Jia, J. Wilson Quail, V.K. Arora, J.R. Dimmock, Acta Crystallogr. C 45 (1989) 285–289.
[3] F.J. Devlin, P.J. Stephens, J. Phys. Chem. A 103 (1999) 527.
[4] M.P. Freitas, C.F. Tormona, R. Rittner, Spectrochim. Acta A 59 (2003) 1177.
[5] P.N. Sobeolev, I.K. Shakrov, R.R. Shagidullin, E.N. Klimovitskii, D.Y. Strel'nik, J. Mol. Struct. 268 (1992) 321.
[6] P.S. Vaz, P.J.A. Ribeiro-Claro, J. Raman Spectrosc. 34 (2003) 863.
[7] S.I. Nam, E.S. Min, Y.M. Jung, M.S. Lee, Bull. Korean Chem. Soc. 22 (2001) 989.
[8] L.D. Barron, J.F. Torrance, J. Urbancich, J. Raman Spectrosc. 13 (1982) 171.
[9] C. James, A. Amal Raj, R. Reghunathan, V.S. Jayakumar, I. Hubert Joe, J. Raman Spectrosc. 37 (2006) 1381.
[10] J. Binoy, A. Amal Raj, R. Reghunathan, I. Hubert Joe, V.S. Jayakumar, J. Comput. Methods Sci. Eng. 7 (2007) 159–173.
[11] L. Padmaja, M. Amalnathan, C. Ravikumar, I. Hubert Joe, Spectrochim. Acta A 74 (2009) 349–356.
[12] K. Udaya Lakshmi, K. Ramamurthi, Cryst. Res. Technol. 40 (2005) 1165.
[13] D. Sajan, J. Binoy, B. Pradeep, K. Venkata Krishna, V.B. Kartha, I. Hubert Joe, V.S. Jayakumar, Spectrochim. Acta 60A (2004) 174.
[14] J. Binoy, J.P. Abraham, I. Hubert Joe, V.S. Jayakumar, G.R. Pettit, O.F. Nielsen, J. Raman Spectrosc. 36 (2005) 63.
[15] D. Sajan, I. Hubert Joe, J. Zaleski, V.S. Jayakumar, Laser Phys. Lett. 2 (2005) 343.
[16] M.J. Frisch, G.W. Trucks, H.B. Schlegel, G.E. Scuseria, M.A. Robb, J.R. Cheeseman, V.G. Zakrzewski, J.A. Montgomery Jr., R.E. Stratmann, J.C. Burant, S. Dapprich, J.M. Millam, A.D. Daniels, K.N. Kudin, M.C. Strain, O. Farkas, J. Tomasi, V. Barone, M. Cossi, R. Cammi, B. Mennucci, C. Pomelli, C. Adamo, S. Clifford, J. Ochterski, G.A. Petersson, P.Y. Ayala, Q. Cui, K. Morokuma, D.K. Malick, A.D. Rabuck, K. Raghavachari, J.B. Foresman, J. Cioslowski, J.V. Ortiz, A.G. Baboul, B.B. Stefanov, G. Liu, A. Liashenko, P. Piskorz, I. Komaromi, R. Gomperts, R.L. Martin, D.J. Fox, T. Keith, M.A. Al-Laham, C.Y. Peng, A. Nanayakkara, M. Challacombe, P.M.W. Gill, B. Johnson, W. Chen, M.W. Wong, J.L. Andres, C. Gonzalez, M. Head-Gordon, E.S. Replogle, J.A. Pople, Gaussian98, A. 9 Revision, Gaussian, Inc., Pittsburgh, PA, 2003.
[17] A.D. Becke, J. Chem. Phys. 98 (1999) 5648.
[18] A.P. Scott, L. Radom, J. Phys. Chem. 100 (1996) 16503.
[19] G. Rahut, P. Pulay, Transferable scaling factors for density functional derived vibrational force fields, J. Phys. Chem. 99 (1995) 3093–3100.
[20] G. Keresztury, S. Holly, J. Varga, G. Besenyei, A.Y. Wang, J.R. Durig, Spectrochim. Acta A 49 (1993) 2007.
[21] J.C. Tai, N.A. Allinge, J. Am. Chem. Soc. 88 (1966) 2179.
[22] H.W. Thomson, P. Torkington, J. Chem. Soc. 171 (1945) 640.
[23] E.D. Glendening, J.K. Badenhoop, A.E. Reed, J.E. Carpenter, J.A. Bohmann, C.M. Morales, F. Weinhold, NBO 5. 0, Theoretical Chemistry Institute, University of Wisconsin, Madison, 2001.
[24] F. Weinhold, Nature 411 (2001) 539.
[25] P. Hobza, Z. Havlas, Chem. Rev. 100 (2000) 4253.
[26] M.S. Weiss, Trends Biochem. Sci. 26 (2001) 521.
[27] P.J.A. Ribeiro-Claro, M.G.B. Drew, V. Felix, Chem. Phys. Lett. 356 (2002) 318.
[28] K. Hermansson, J. Phys. Chem. A 106 (2002) 4695.
[29] H. Sato, J. Dybal, R. Murakami, I. Noda, Y. Ozaki, J. Mol. Struct. 744 (2005) 35.
[30] Y. Yang, W. Zhang, X. Gao, Int. J. Quantum Chem. 106 (2006) 1199.
[31] P. Politzer, D.G. Truhlar (Eds.), Chemical Applications of Atomic and Molecular Electrostatic Potentials, Plenum Press, New York, 1981.
[32] C.H. Choi, M. Kertesz, J. Phys. Chem. A 101 (1997) 3823.
[33] G. Varsanyi, Vibrational Spectra of Benzene Derivative, Academic Press, New York, 1969.
[34] N.B. Colthup, L.H. Daly, S.E. Wiberley, Introduction to Infrared and Raman Spectroscopy, Academic Press, New York, 1990.
[35] F.R. Dollish, W.G. Fateley, F.F. Bentley, Characteristic Raman Frequencies of Organic Compounds, John Wiley & Sons, New York, 1997.

[36] G. Socrates, Infrared Characteristic Group frequencies, Wiley-Interscience Publication, New York, 1980.
[37] B. Smith, Infrared Spectral Interpretation, A Systematic Approach, CRC Press, Washington, DC, 1999.
[38] H. Speeding, D.H. Wiffen, Proc. Roy. Soc. Lond. A 238 (1956) 245.
[39] M. Tasumi, T. Urano, M. Nakata, J. Mol. Struct. 146 (1986) 383–396.
[40] A. Purkayastha, K. Kumar, Spectrochim. Acta A 43 (1987) 1269.
[41] J.C. Tai, N.L. Allinger, J. Am. Chem. Soc. 88 (1966) 2179.
[42] Y. Huang, D.F.R. Gilson, I.S. Butler, J. Phys. Chem. 97 (1993) 1998.